ELSEVIER

Surface Science 490 (2001) 308–314

SURFACE SCIENCE

www.elsevier.com/locate/susc

# Surface plasmon effects on surface second harmonic generation during Au nanoparticle deposition onto H–Si(1 1 1)

Ramanathan Srinivasan, Yuan Tian, Ian Ivar Suni *

*Department of Chemical Engineering, Clarkson University, Potsdam, NY 13699-5705, USA*

Received 8 November 2000; accepted for publication 7 May 2001

**Abstract**

Deposition of Au nanoparticles from aqueous HF onto H–Si(1 1 1) was studied in situ by surface second harmonic generation (SHG) and ex situ by extinction spectroscopy and non-contact atomic force microscopy (AFM). AFM measurements indicate that the maximum SHG intensities occur at lateral particle diameters of approximately 90–100 nm independent of solution phase composition, but with an intensity that depends on solution phase composition.

Employing the evolution of SHG intensity to monitor lateral cluster growth, simultaneous Au deposition and Si oxidation exhibit apparent kinetic reaction orders of $1/2$ and zero with respect to HF and $Au(CN)_2^-$, respectively. These results are similar to those obtained purely from ex situ AFM analysis. The variations in SHG intensity with $Au(CN)_2^-$ concentration can be related to particle nucleation densities. These results demonstrate the utility of SHG as an in situ probe of particle growth. © 2001 Published by Elsevier Science B.V.

*Keywords:* Models of non-linear phenomena; Models of surface kinetics; Atomic force microscopy; Non-linear optical methods; Second harmonic generation methods; Second harmonic generation; Surface chemical reaction; Gold; Silicon; Single crystal surfaces; Solid–liquid interfaces

## 1. Introduction

Due to their low resistivity and good corrosion resistance, noble metal thin films have a variety of applications as contacts and conductors in the electronics industries [1–5]. When feasible, noble metal deposition by electrochemical means is usually desirable as it is less expensive than vacuum methods. On the other hand, direct noble metal deposition onto Si during wafer cleaning and preparation prior to semiconductor device fabrication is undesired and must be prevented to maintain high device yields. Following dissolution of the native $SiO_x$ oxide in aqueous HF, noble metals may be reduced and deposited onto bare Si, which is a strong reducing agent [6].

Metal deposition from aqueous HF initially forms nm-sized particles that are approximately oblate hemispheroids, as seen by scanning probe microscopy [7–11]. Such noble and alkali metal nanoparticles exhibit strong resonant electric field enhancements associated with the surface plasmon resonance, producing highly colored colloidal solutions [12,13].

Electric field enhancements in surface ensembles of noble and alkali metal nanoparticles can also

* Corresponding author. Tel.: +1-315-268-5705/4471; fax: +1-315-268-6654.

*E-mail address:* isuni@clarkson.edu (I.I. Suni).

0039-6028/01/$ - see front matter © 2001 Published by Elsevier Science B.V.
PII: S0039-6028(01)01350-4

produce strong signal enhancements during surface-enhanced Raman spectroscopy (SERS) and surface second harmonic generation (SHG) [14–18]. Although such enhancements are readily observable, the detailed relationship between the signal magnitude and the particle size and shape is quite complex. Several groups have recently studied surface SHG in situ during growth of metal nanoparticles on insulating or semiconducting substrates [19–27]. The present report details studies of the relationship between surface SHG and the size and density of Au nanoparticles deposited from HF onto Si(1 1 1) by galvanic displacement.

## 2. Experimental

Prior to each experiment, the p-type 0.01 Ω cm Si(1 1 1) sample was cleaned by immersion into a 0.50 M HF etchant and typical SC-1 ($H_2O$:$H_2O_2$:$NH_4OH$) and SC-2 ($H_2$:$H_2O_2$:HCl) cleaning solutions. Hydrogen-terminated H–Si(1 1 1) was subsequently prepared by immersion into 0.50 M HF and is known to be stable for hours. The $SiO_x$ oxide layer is removed in this manner to separate the deposition kinetics of Au from the complex dissolution kinetics of the native oxide.

Au was deposited from aqueous solutions containing different concentrations of $KAu(CN)_2$ and HF, with the pH ranging from 0.4 to 1.9. The experimental setup for in situ surface SHG measurements has been previously described [27]. The pump laser is a Continuum Powerlite 6050 Nd:YAG laser operating at 1064 nm and 50 Hz and the detector a gated, intensified Princeton Instruments LN/1024 CCD. The pump laser was polarized perpendicular to the plane of incidence. Previous investigators have found that ns-laser irradiation may cause desorption from insulating substrates [19,23]. However, control experiments showed that a pump laser fluence of 5 mJ/pulse did not affect the metal clusters, probably due to the low absorptivity of Si at 1064 nm.

Accurate in situ extinction spectroscopy is difficult in this system due to drift in the optical components over the experimental timescale. A stable reference is needed to subtract the effects of the Si substrate, and this was provided by a freshly prepared H–Si(1 1 1) surface. For this reason, ex situ visible–ultraviolet extinction spectroscopy was performed in reflection mode following sample emersion with:

$$\gamma = \frac{I_{Si} - I_{Au/Si}}{I_{Si}} \tag{1}$$

Following emersion, the Au/Si substrate and the H-terminated Si reference were affixed to an optical mount so that they could be rapidly interchanged.

Ex situ atomic force microscopy (AFM) images were also obtained for a variety of different conditions following sample emersion. AFM images were obtained in non-contact mode to prevent particle displacement [11]. In this mode the cantilever oscillates near its resonance frequency with a small amplitude, and the frequency and amplitude of the oscillation may be altered when the tip interacts with the sample. During imaging, the oscillation amplitude is held constant. All reported statistics are averages of at least three AFM images. The tip diameter of 10 nm has been subtracted from all reported values.

## 3. Results

Deposition of Au from aqueous HF by galvanic displacement of Si can be described by the following overall half reactions,

$$Au(CN)_2^- + e^- \rightarrow Au + 2CN^- \tag{2}$$

$$Si + 6HF \rightarrow SiF_6^{2-} + 6H^+ + 4e^- \tag{3}$$

The growth of Au nanoparticles on the Si surface yields SHG enhancement due to resonance of the second harmonic photon (532 nm) with the Au surface plasmon. The variation of the SHG intensity with time and HF concentration has previously been reported during Au deposition onto H–Si(1 1 1) from solutions containing $10^{-4}$ M $KAu(CN)_2$ [27]. The association of maxima in the SHG intensity with cluster diameters of approximately 100 nm and the dependence of these maxima on the concentration of the various

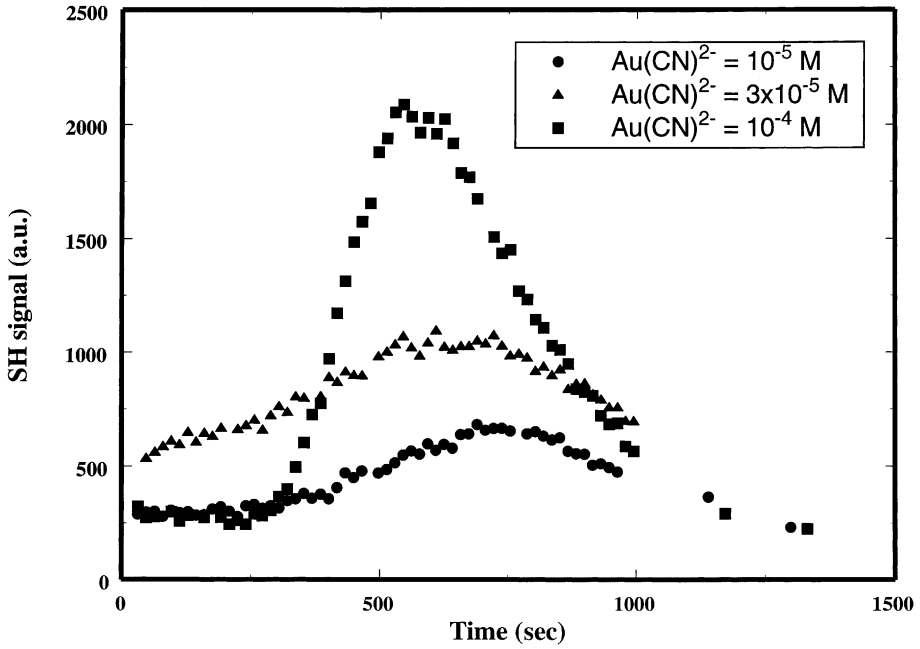


Fig. 1. Second harmonic signal as a function of time during Au deposition from 0.050 M HF at various $KAu(CN)_2$ concentrations.

fluoride-containing species allowed a series of experiments to identify HF as the mechanistically active species towards Si oxidation with an apparent reaction order of 1/2 [11,27].

Fig. 1 shows the results of an in situ study of the effects of the $Au(CN)_2^-$ concentration on the temporal evolution of the SHG intensity during Au nanoparticle deposition from 0.5 M aqueous HF. The times at which the SHG maxima occur depend only weakly on $Au(CN)_2^-$ concentration, but the intensities of the maxima increase rapidly with increasing concentration.

These results differ from those reported previously, where the time at which the maximum occurs depends strongly on HF concentration [27]. If the results of Fig. 1 are extended to long times so that continues Au films are deposited, the SHG intensity rises again, and the final intensity is approximately 2.4× greater than that from the bare H–Si(1 1 1) surface.

Ex situ extinction spectra were also obtained to investigate the evolution of the surface plasmon resonance with Au nanoparticle size. Fig. 2 shows the results for Au nanoparticle deposition from $10^{-4}$ M $KAu(CN)_2$ and 0.50 M HF. The extinction spectra exhibit maxima near 550–600 nm, with the maximum red-shifting with time, then eventually declining in intensity. In general, the overall extinction intensity increases and declines with Au nanoparticle growth in parallel to the SHG signal at 532 nm.

AFM images were obtained at several different times for each of the three solutions included in Fig. 1, and the nanoparticles are approximately oblate hemispheroids as expected. Analysis of the AFM images shows clearly that nucleation is progressive in this system [28]. Although this result might be considered surprising given the long time scales relative to most studies of electrochemical nucleation, the overpotentials involved in electroless processes are often modest. It should be noted that traditional electrochemical nucleation experiments are not feasible for this system due both to the inability to electrodeposit Au onto p-type Si and to likely interference from hydrogen evolution. Despite the resulting heterogeneous cluster size distribution, one can show that the average cluster size follows the same phenomenological

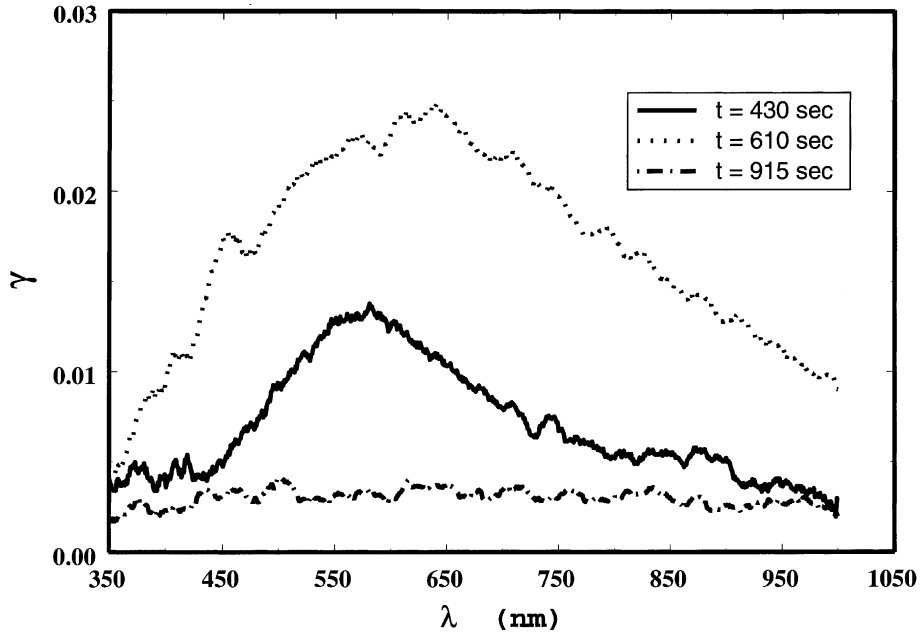


Fig. 2. Extinction spectra of Au nanoparticles deposited from 0.50 M HF and $10^{-4}$ M $KAu(CN)_2$.

rate law as individual clusters. However, the prefactor for the growth of the average cluster size is altered from that for individual clusters.

In agreement with previous results, the SHG maxima in Fig. 1 can be associated with particle size of 90–100 nm [11,27]. Fig. 3 shows ex situ non-contact AFM images of Au nanoparticles at the times for which the SHG intensities in Fig. 1 reach maxima. Statistical analysis of AFM images taken at these maxima yield average cluster diameters of 91, 93 and 94 nm for deposition from $10^{-5}$, $3 \times 10^{-5}$, and $10^{-4}$ M $KAu(CN)_2$ respectively, and average cluster heights of 3–7 nm. The nucleation densities at the SHG maxima are approximately $5.0 \times 10^8$, $9.8 \times 10^8$ and $1.6 \times 10^9$ $cm^{-2}$, respectively.

## 4. Discussion

Perhaps the most interesting result of the current study is the observation that the maximum SHG intensity occurs for cluster arrays of approximately 90–100 nm average lateral diameter. The origin of this maximum and the relationship of the surface plasmon-enhanced SHG intensity to the Au nanoparticle size and shape is fairly complex. In general agreement with the current results, studies of electrochemically roughened Au electrodes by in situ SERS and ex situ AFM demonstrated that Au features of about 100 nm size yield the maximum SERS enhancement of the pyridine ring-breathing mode [29]. For spherical Au colloids, the maximum absorbance at 532 nm occurs for particles of approximately 60–80 nm diameter [12,13], slightly below the size range seen in the current study. Recently surface SHG from Na nanoparticles grown on dielectric substrates in vacuum has been studied as a function of cluster size, and maxima similar to those in Fig. 1 have been observed [22–24].

The surface plasmon resonance typically occurs in the range 510–540 nm for spherical Au nanoparticles and is red-shifted for large particles [30–32]. However, for spheroidal particles, the dipolar surface plasmon resonance typically splits into two components, one blue- and the other red-shifted, arising from excitation along the major and minor axes, respectively. Although supportive of the significant surface plasmon enhancements seen in the SHG results, the extinction spectra shown in

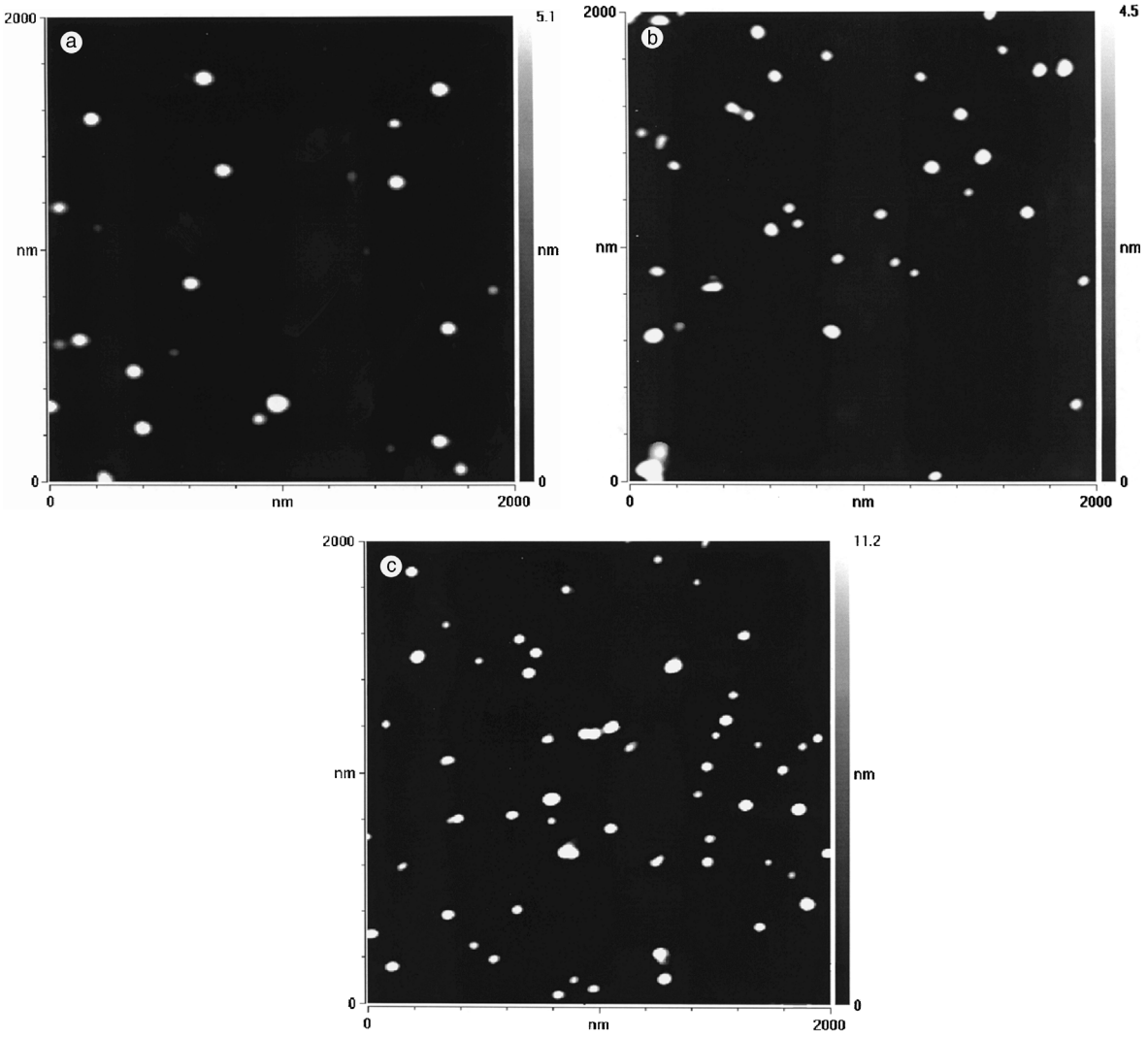


Fig. 3. Non-contact AFM image of Au nanoparticles at the maximum in Fig. 1 for (a) $10^{-5}$ M $KAu(CN)_2$, (b) $3 \times 10^{-5}$ M $KAu(CN)_2$ and (c) $10^{-4}$ M $KAu(CN)_2$.

Fig. 2 differ from those expected, since maxima occur close to the typical surface plasmon resonance for spherical Au particles. It should be noted that the distribution of aspect ratios for all experiments discussed here is not nearly broad enough to account for the unusual extinction maximum. In all cases, no particles are imaged by AFM with aspect ratios above approximately 0.30.

The non-zero baseline in Fig. 2 may be associated with the choice of a reference substrate. The existence of monolayer and multilayer films of AuCN have been proposed in this system [33,34], with evidence for substantial inclusion of AuCN in the final Au deposit [35]. Clearly the presence of such films will affect the measured extinction spectra. The ability to obtain surface SHG spectra in situ and their relatively ''backgroundless'' nature in this resonant system make SHG much more appropriate than extinction spectroscopy for studies of Au nanoparticle growth.

The changes in the surface plasmon resonance with increasing particle size have not been well

studied for hemispheroids. The intensity of the dipolar surface plasmon resonance of spherical nanoparticles is expected to rise with particle volume until the particle size becomes significant with respect to the wavelength of light. At this point retardation effects cause the dipolar surface plasmon to red-shift and decline in intensity. Simultaneously, quadrupole and higher order multipoles begin to contribute significantly to surface plasmon effects. This can be seen clearly in the absorbance and extinction spectra of spherical Ag nanoparticles larger than about 100 nm diameter [36–38]. While the dipole resonance red-shifts with increasing particle size, the quadruapole and higher multipoles remain close to the wavelength of the original dipole resonance.

The size at which the maximum SHG intensity occurs can be employed to probe the kinetics of Au nanoparticle growth. Volmer–Weber growth kinetics during vacuum deposition have been thoroughly studied. However, the existence of adsorption isotherms and electrocatalytic effects, which may be more important than relative interfacial energies, make electrochemical particle growth more complex. Clearly the exchange current density for both the anodic and cathodic reactions will be much higher on Au than on Si.

For these reasons, a phenomenological kinetic analysis is performed based on

$$\text{Lateral growth rate} \propto [\mathrm{HF}]^{\alpha}[\mathrm{Au(CN)}_2^-]^{\beta}, \qquad (4)$$

where $\alpha$ and $\beta$ are apparent reactions orders with respect to the two reactants. The apparent reaction order differs from a true reaction order in that growth is only being considered in two dimensions. Previous results showed that HF was the active species with respect to Si oxidation with $\alpha \approx 1/2$ [27]. Using the temporal maximum in the SHG signal as a measure of growth rate, a similar analysis for the present results yields $\beta \approx 0.1$.

One must hesitate to make firm kinetic conclusions based on a limited data set. However, further variations in the concentration of $Au(CN)_2^-$ are limited by particle coalescence at high concentration and by signal intensity at low concentration. In support of the present conclusion, independent AFM image analysis yields a similar reaction order ($\alpha = 0.06$) [28]. This indicates that the lateral particle growth rate is independent of the $Au(CN)_2^-$ concentration, suggesting that an excess of Au(I) species is available for nanoparticle growth. These results demonstrate the utility of SHG as an in situ probe of particle growth.

The origin of the relative SHG intensities at the maxima in Fig. 1 mainly reflects differences in the nucleation density, although the aspect ratios may also have some effect. The average nucleation densities from AFM images at the SHG maxima for $3 \times 10^{-5}$ and $10^{-4}$ M $KAu(CN)_2$ relative to those for $10^{-5}$ M $KAu(CN)_2$ are 2.0 and 3.2, respectively. Similarly, the relative SHG enhancements at the corresponding maxima in Fig. 1 are 1.6 and 3.1, respectively. Thus, the relative nucleation density closely matches the relative SHG enhancement. However, this may not be generally be the case. Previous results suggest that in some cases Au nanoparticle aspect ratio may also affect the relative SHG intensities [27].

## Acknowledgements

This research has been supported by NSF grant CTS-9527497. Thanks to George C. Schatz and Richard P. van Duyne for helpful discussions.

## References

[1] P.L. Pai, C.H. Ting, IEEE Electron. Dev. Lett. 10 (1989) 423.
[2] J. Tao, N.W. Cheung, C. Hu, H.K. Kang, S.S. Wong, IEEE Electron. Dev. Lett. 13 (1992) 433.
[3] J. Tao, N.W. Cheung, C. Hu, IEEE Electron. Dev. Lett. 14 (1993) 249.
[4] J. Kim, S.H. Wen, D.Y. Jung, R.W. Johnson, IBM J. Res. Develop. 28 (1984) 697.
[5] M. Matsuoka, J. Murai, C. Iwakura, J. Electrochem. Soc. 139 (1992) 2466.
[6] F. Kern, M. Itano, I. Kawanabe, M. Miyashita, R. Rosenberg, T. Ohmi, Proceedings, Ultra Clean Society 11th Workshop on ULSI Ultraclean Technology, Tokyo, Japan, 6 June, 1991, p. 23.
[7] H. Morinaga, M. Suyama, T. Ohmi, J. Electrochem. Soc. 141 (1994) 2834.
[8] O.M.R. Chyan, J.J. Chen, H.Y. Chien, J. Sees, L. Hall, J. Electrochem. Soc. 143 (1996) 92.
[9] M.K. Lee, J.J. Wang, H.D. Wang, J. Electrochem. Soc. 144 (1997) 1777.

[10] L.A. Nagahara, T. Ohmori, K. Hashimoto, A. Fujishima, J. Vac. Sci. Technol. A 11 (1993) 763.
[11] C. Rossiter, I.I. Suni, Surf. Sci. 430 (1999) L553.
[12] G. Mie, Ann. Phys. 25 (1908) 377.
[13] J. Turkevich, G. Garton, P.C. Stevenson, J. Coll. Sci. Suppl. 1 (1954) 26.
[14] S.S. Wang, M. Kerker, Phys. Rev. B 24 (1981) 1777.
[15] J. Gersten, A. Nitzan, J. Chem. Phys. 75 (1981) 1139.
[16] P.W. Barber, R.K. Chang, H. Massoudi, Phys. Rev. B 27 (1983) 7251.
[17] C.K. Chen, T.F. Heinz, D. Ricard, Y.R. Shen, Phys. Rev. B 27 (1983) 1965.
[18] E.J. Zeeman, G.C. Schatz, J. Phys. Chem. 91 (1987) 634.
[19] A. Wokaun, J.G. Bergman, J.P. Heritage, A.M. Glass, P.F. Liao, D.H. Olsen, Phys. Rev. B 24 (1981) 849.
[20] G.T. Boyd, T. Rasing, J.R.R. Leite, Y.R. Shen, Phys. Rev. B 30 (1984) 519.
[21] O.A. Aktsipetrov, P.V. Elyutin, A.A. Fedyanin, A.A. Nikulin, A.N. Rubtsov, Surf. Sci. 325 (1995) 343.
[22] T. Gotz, M. Buck, C. Dressler, F. Eisert, F. Trager, Appl. Phys. A 60 (1995) 607.
[23] T. Muller, P.H. Vaccaro, F. Balzer, H.G. Rubahn, Opt. Commun. 135 (1997) 103.
[24] J.H. Klein-Wiele, P. Simon, H.G. Rubahn, Phys. Rev. Lett. 80. (1997) 45.
[25] M. Simon, F. Trager, A. Assion, B. Lang, S. Voll, G. Gerber, Chem. Phys. Lett. 296 (1998) 579.
[26] R. Srinivasan, I.I. Suni, Surf. Sci. 408 (1998) L698.
[27] R. Srinivasan, I.I. Suni, J. Electrochem. Soc. 146 (1999) 170.
[28] Y. Tian, I.I. Suni, J. Electrochem. Soc., submitted for publication.
[29] A.G. Brolo, D.E. Irish, G. Szymanski, J. Lipkowski, Langmuir 14 (1998) 517.
[30] T.S. Ahmadi, S.L. Logunov, M.A. El-Sayed, J. Phys. Chem. 100 (1996) 8053, references therein.
[31] Y. Cheng, D.J. Schiffrin, J. Chem. Soc. Faraday Trans. 92 (1996) 3865, references therein.
[32] J.P. Wilcoxon, R.L. Williamson, R. Baughman, J. Chem. Phys. 98 (1993) 9933, references therein.
[33] E.T. Eisenmann, J. Electrochem. Soc. 125 (1978) 717.
[34] Y.G. Li, A. Lasia, J. Electrochem. Soc. 144 (1997) 1979.
[35] G. Holmbom, B.E. Jacobson, J. Electrochem. Soc. 135 (1989) 787.
[36] B.K. Russell, J.G. Mantovani, V.E. Anderson, R.J. Warmack, T.L. Ferrell, Phys. Rev. B 35 (1987) 2151.
[37] U. Kreibig, B. Schimtz, H.D. Breuer, Phys. Rev. B 36 (1987) 5027.
[38] T. Jensen, L. Kelly, A. Lazarides, G.C. Schatz, J. Clust. Sci. 10 (1999) 295.